Available online at www.sciencedirect.com

jmr&t Journal of Materials Research and Technology

journal homepage: www.elsevier.com/locate/jmrt

Short Communication

Enhanced pitting resistance through designing a high-strength 316L stainless steel with heterostructure

Jiansheng Li [a,b,*,1], *Qingzhong Mao* [d,1], *Ming Chen* [a,b], *Wenbo Qin* [c,**], *Xianke Lu* [a,b], *Tong Liu* [a,b,f], *Dingshun She* [c,e], *Jiajie Kang* [c,e], *Gang Wang* [a,b], *Xiebin Zhu* [a,b], *Yusheng Li* [d]

[a] *School of Materials Science and Engineering, Anhui Polytechnic University, Wuhu, 241000, PR China*
[b] *Anhui Key Laboratory of High-Performance Non-ferrous Metal Materials, Anhui Polytechnic University, Wuhu, 241000, PR China*
[c] *School of Engineering and Technology, China University of Geosciences (Beijing), Beijing, 100083, PR China*
[d] *Nano and Heterogeneous Materials Center, School of Materials Science and Engineering, Nanjing University of Science and Technology, Nanjing, 210094, PR China*
[e] *Zhengzhou Institute, China University of Geosciences (Beijing), Zhengzhou, 451283, PR China*
[f] *HIT-Chungu Joint Research Center for Additive Manufacturing Materials, Anhui Chungu 3D Printing Institute of Intelligent Equipment and Industrial Technology, Wuhu, Anhui, 241200, PR China*

ARTICLE INFO

Article history:
Received 13 September 2020
Accepted 4 December 2020
Available online 9 December 2020

Keywords:
316L stainless steel
Heterostructure
EBSD
Pitting resistance
Potentiodynamic polarization

ABSTRACT

A high-strength 316L stainless steel with heterostructure (HS) was used to explore its corrosion properties in 3.5wt.% NaCl solution at 25 °C. Compared with a conventional coarse-grained (CG) sample, the HS sample with the characteristic of that the recrystallized grains (RGs) were surrounded by ultrafine/nano-structures (UFS/NSs) exhibited an enhanced pitting resistance. This was ascribed to interrupted propagation of the stable corrosion pits in RGs by the surrounded UFS/NSs. The results in current work may provide a new strategy to improve corrosion properties by heterostructural designing.

* Corresponding author.
** Corresponding author.
E-mail addresses: drlijiansheng@163.com, lijiansheng@ahpu.edu.cn (J. Li), qwb_strive@126.com (W. Qin).
[1] These authors contributed equally to this work.

https://doi.org/10.1016/j.jmrt.2020.12.005

1. Introduction

316L austenitic stainless steel has a wide application in coastal instruments because of its excellent corrosion behaviour and good mechanical properties [1–3]. However, pitting corrosion often occurs when it is immersed in the natural sea water, which includes high concentrations of chloride ion, leading to the accelerated failure of coastal instruments [4,5]. In the past several decades, researchers had paid much attention to explore the initiation and propagation processes of corrosion pits, so as to reveal the pitting mechanisms of coarse-grained (CG) and ultrafine/nano-grained 316L mechanical parts [6,7]. Many previous references [8–10] pointed out that corrosion pits were preferred to initiate at the grain boundaries and edge of MnS inclusions in a CG 316L sample, and only the stable pits (absence of passive film) can grow steadily during the whole corrosion process. As compared with the CG sample, ultrafine/nano-grained samples always exhibited improved pitting resistance because of the easy formation of positive passive film. Hajizadeh et al. [7] as well as Zheng and Zheng [11] indicated that the growth rate of passive film can be accelerated on the ultrafine/nano-structure(UFS/NS) surface. This was because the small grains promoted the formation of Cr-rich passive layer by increasing the diffusion rate of Cr, and thereby enhancing their pitting resistance. Recently, many eye-catching heterostructured (HS) stainless steels, consisted of the mixtures of recrystallized grains (RGs) and UFS/NS, are frequently reported to exhibit remarkable mechanical and tribological properties [12–16]. However, their corrosion properties are rarely explored, especially the coordination corrosion mechanism around hetero-interfaces. Thus, it is necessary to study the corrosion behaviours in relation to their hetero-microstructures, which may provide a scientific cognition of the corrosion mechanisms for HS metallic materials.

In this work, a novel high-strength HS 316L stainless steel (yield strength of ~1 GPa [13,14]) has been selected and systematically reveal its corrosion behaviour and pitting mechanism in 3.5 wt.% NaCl solution at 25 °C.

2. Experimental details

The original CG 316L sample with average grain size of ~40 μm has a chemical composition (in wt.%) of Cr-16.47, Ni-10.10, Mo-1.97, C-0.03, P-0.03, S-0.005, Si-0.53, Mn-1.42, Nb-0.01, Co-0.24, Cu-0.15, W-0.03 and Fe-balance. The present HS 316L sample with the mixed microstructures of RGs and UFS/NSs was prepared through severe rolling deformation and annealing as introduced in details in our previous work [14].

Electrochemical corrosion behaviors of CG and HS 316L samples (with the working area of 1 cm^2) in 3.5 wt.% NaCl solution were performed by using a VERSCAN electrochemical testing system in a traditional three-electrode cell. The saturated calomel electrode (SCE), platinum electrode and 316L sample were used as reference electrode, counter electrode and working electrode, respectively. Before the electrochemical measurements, all the test surfaces of the present 316L samples were firstly ground with 1200 grit SiC papers and then polished by a 50-nm colloidal silica slurry, which was aimed to obtain ideal smooth surfaces and avert any effect from surface roughness on pitting corrosion. Following the slurry polishing, all the 316L samples were ultrasonically cleaned in ethanol and deionized water for 30 min and dried in air. Potentiodynamic polarization tests started after the 1.5-h immersion for allowing the samples to reach stable states. The potentiodynamic polarization test was performed at 25 °C in the applied potential with a scan rate of 1 $mV \cdot s^{-1}$ scanning from −500 mV (vs open circuit potential, OCP) to 1000 mV (vs OCP). The ratio of the volume of NaCl solution to the working surface area was 200 $ml \cdot cm^{-2}$. To guarantee the reproducibility of the obtained results, all the potentiodynamic polarization curves were measured three times.

The austenitic and martensitic phases in CG and HS 316L samples were analyzed by a Bruker-AXS D8 Advance X-ray diffractometer (XRD) using the Cu Ka radiation. The scanning speed was 6°/min and 2-Theta ranged from 40° to 100°. Field emission scanning electron microscopy (FEG/SEM), in a Quant 250 FEG microscope, was used to capture the morphologies of corrosion pits on the ND and TD surfaces. The microstructures after potentiodynamic polarization tests with various terminal potentials were examined through an electron backscattered diffraction (EBSD). The step size was 20–2000 nm and the scanning voltage was 15 kV. The microstructures of present HS 316L sample were observed based on a TECNAI G2 20 LaB6 transmission electron microscope (TEM) at 200 kV.

3. Results and discussion

As presented in Fig. 1, the CG sample displays a homogeneous microstructure with the average grain size of ~40 μm while the HS sample displays a heterogeneous microstructure that the RGs are surrounded by UFS/NSs. Both the CG and HS samples are composed of a single austenitic phase. The detailed microstructured information has been introduced in our previous works [14].

Fig. 2a presents the potentiodynamic polarization plots of CG and HS samples. It indicates that present HS sample exhibits a superior pitting resistance than that of CG sample as reflected by the increased pitting potential (E_P) from 320 to 425 mV. The corrosion potential (Ecorr)/corrosion current density (Icorr) of CG and HS samples are −263 mV/3×10^{-7} $A \cdot cm^{-2}$ and -8 mV/1.9×10^{-8} $A \cdot cm^{-2}$, respectively. As revealed in Fig. 2b and c, the mild pitting morphology with plenty of metastable pits directly confirms the better pitting resistance of HS sample. This may indicate that the HS sample has a broad application prospect in the future.

In the current work, the pitting initiation and propagation processes in CG and HS samples are compared with each other based on the EBSD results in Fig. 3 and Fig. 4, which is aimed to reveal the pitting mechanism and enhanced pitting

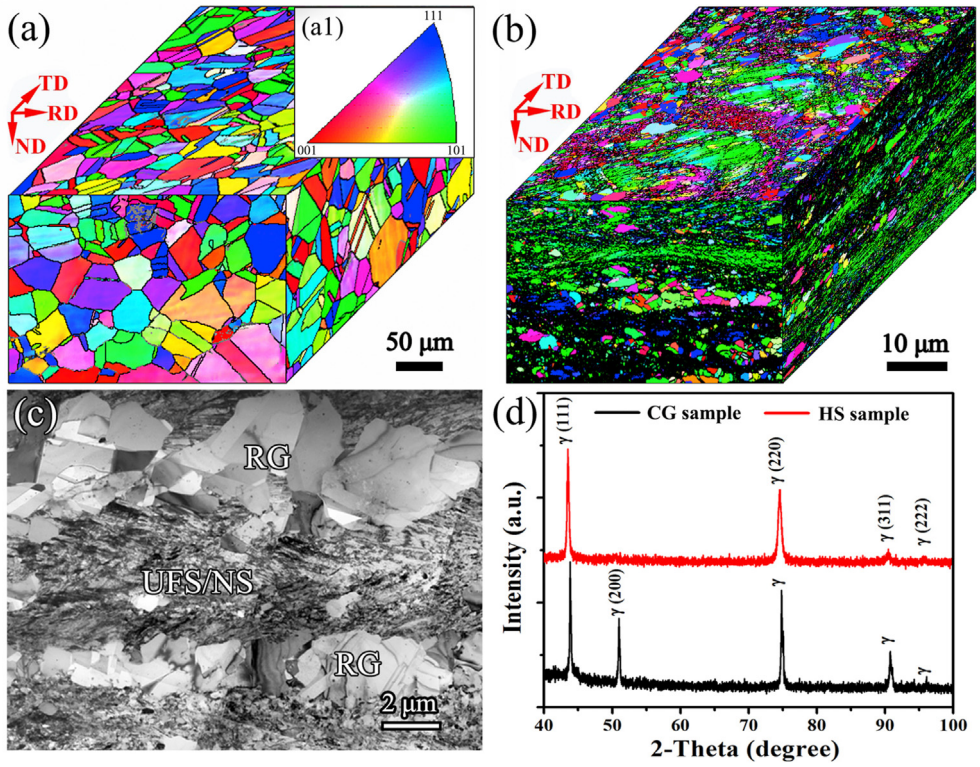

Fig. 1 – (a) and (b) are the microstructures of CG and HS samples, where the ND, TD and RD refer to normal direction, transverse direction and rolling direction; (c) TEM image of HS sample (TD plane); (d) [12] XRD curves of CG and HS samples.

resistance of HS sample. As displayed in Fig. 3a–c and Fig. 4a–c, it is confirmed that corrosion pits both on the CG and HS sample surfaces are inclined to initiate around the grain boundaries. This is attributed to that more nucleation points can be easily provided by grain boundaries with numerous defects instead of the interior of the grains [8,17]. Unfortunately, the initiated corrosion pits rapidly propagate across the grains when gradually increases of polarization potential, and eventually generate many macro/micro-size pits on the surfaces of CG sample surface (Fig. 2b, Fig. 3d–i). For the HS sample, only the initiated corrosion pits around RGs can be transferred into stable pits to form the micro-size corrosion pits (Fig. 2c, Fig. 4d–f). Taking into consideration of the present results and previous references [1,7,11,18], the pitting mechanism and enhanced pitting resistance of HS sample can be explained by Fig. 5. The enhanced pitting resistance could be related to the fast metastable pitting initiation and re-passivation by a thicker passive layer with a

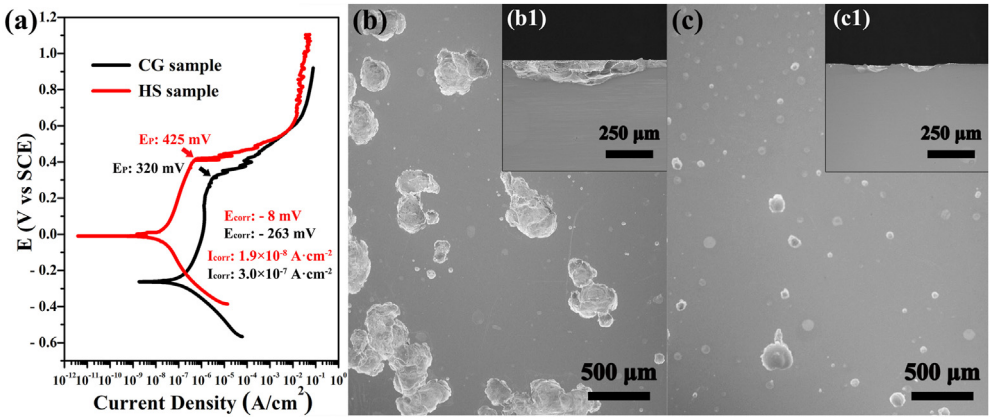

Fig. 2 – (a) Potentiodynamic polarization plots of CG and HS samples; (b) and (c) are the SEM surface morphologies (ND plane) of tested CG and HS samples, where the (b1) and (c1) show the cross-sectional images of corrosion pits in (b) and (c).

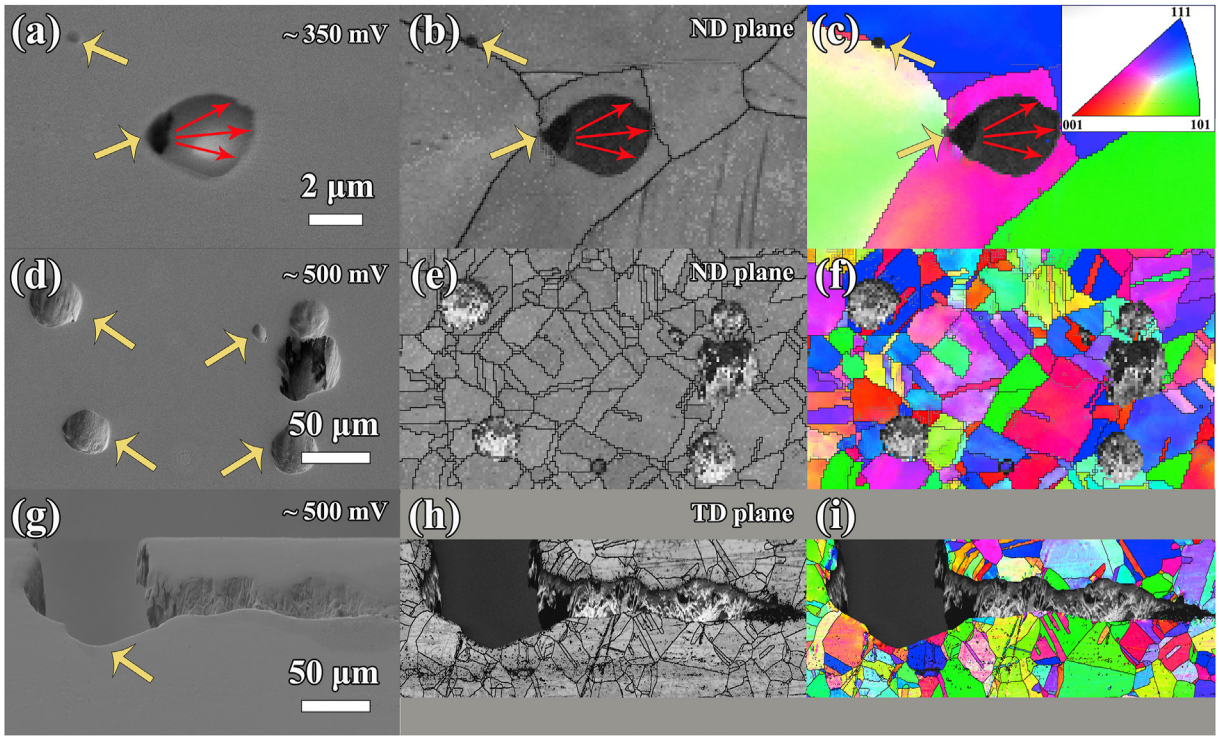

Fig. 3 – (a), (d) and (g) are the SEM images of corrosion pits of CG samples after potentiodynamic polarization tests, (a) ND surface at ~350 mV, (d) ND surface at ~500 mV, (g) TD surface at ~500 mV; (b), (e) and (h) are corresponding EBSD contrast images of (a), (d) and (g); (c), (f) and (i) are corresponding EBSD IPF images of (a), (d) and (g).

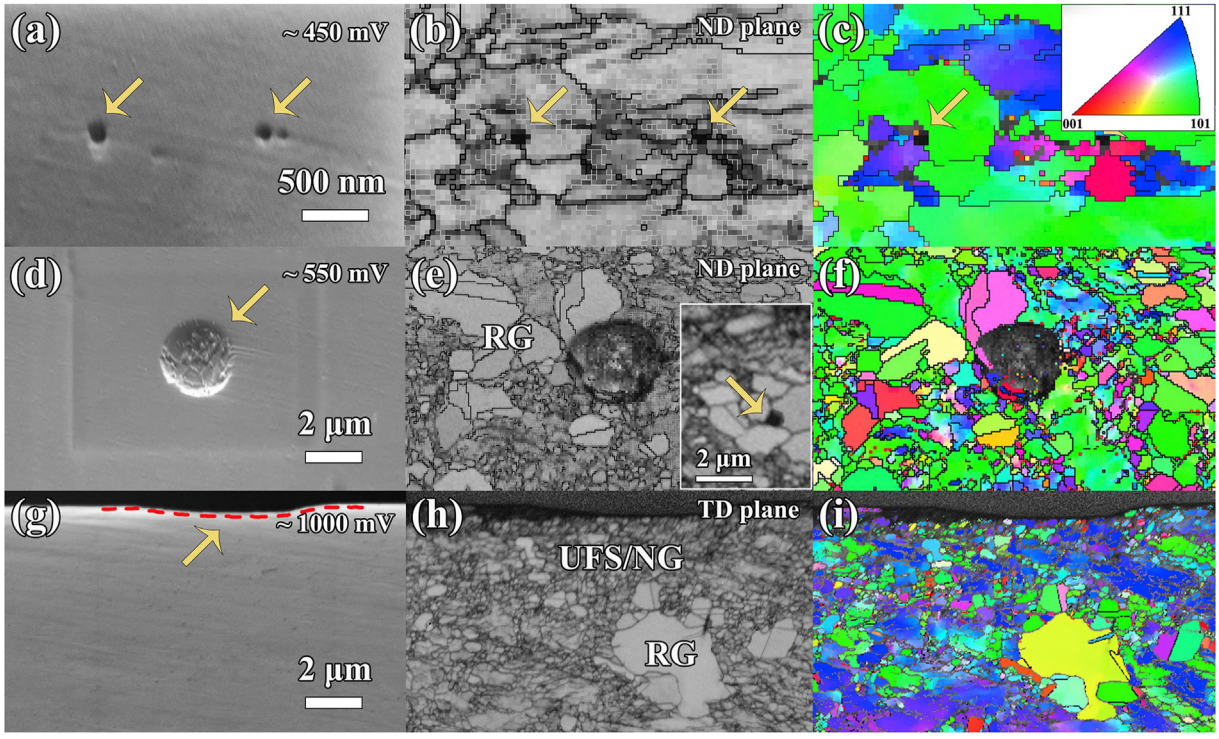

Fig. 4 – (a), (d) and (g) are the SEM images of corrosion pits of HS samples after potentiodynamic polarization tests, (a) ND surface at ~450 mV, (d) ND surface at ~550 mV, (g) TD surface at ~1000 mV; (b), (e) and (h) are corresponding EBSD contrast images of (a), (d) and (g), where the inset in (e) indicates the initiation of corrosion pit in RGs; (c), (f) and (i) are corresponding EBSD IPF images of (a), (d) and (g).

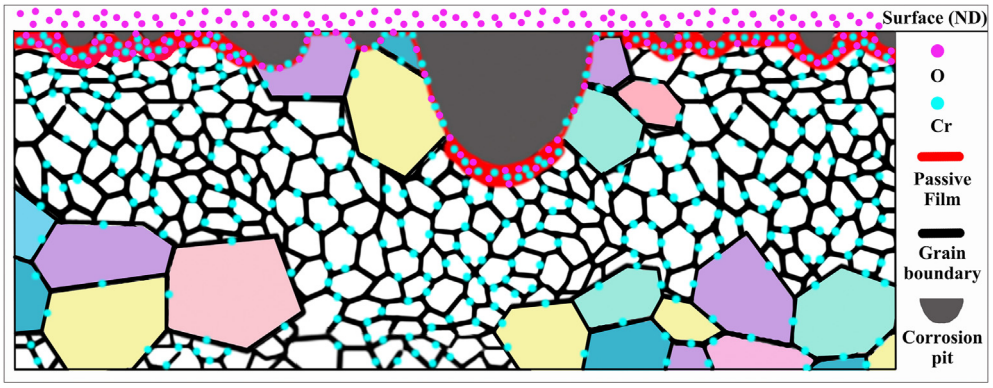

Fig. 5 – Schematics presenting the initiation and propagation of corrosion pits on the surface of HS sample.

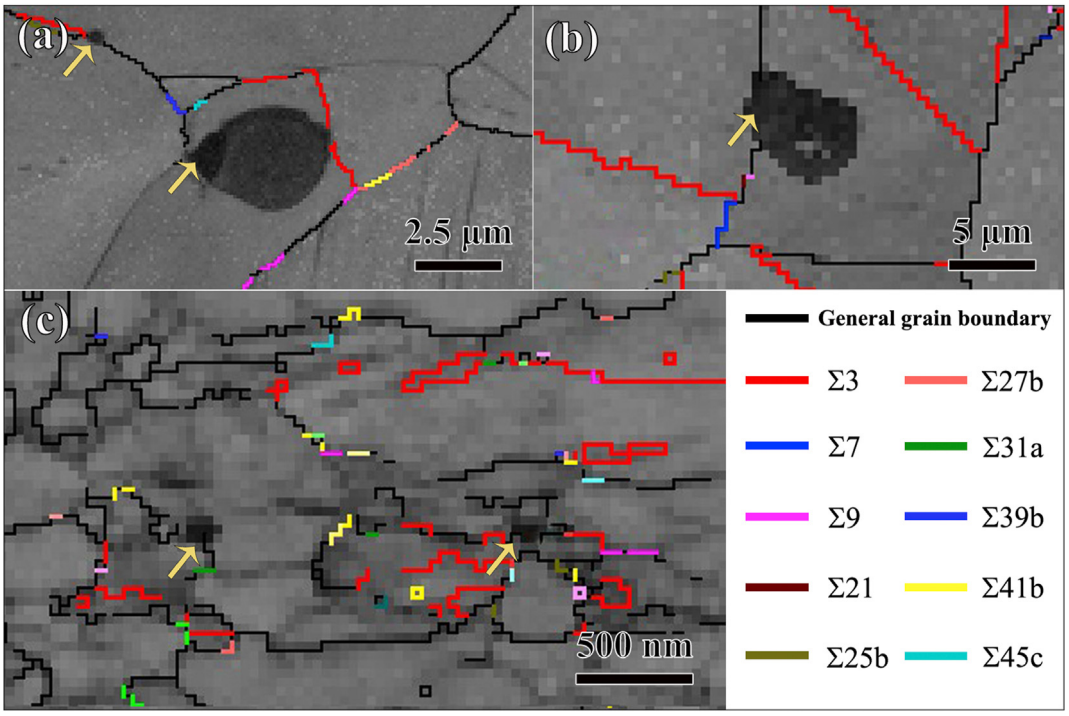

Fig. 6 – (a) and (b) are the EBSD contrast images of the corrosion pits on the CG sample surface after potentiodynamic polarization tests at ~350 mV; (c) is the EBSD contrast image of the corrosion pits on the HS sample surface after potentiodynamic polarization test at ~450 mV. It is noted that the general grain boundary and ∑coincidence site lattice (∑CSL) boundaries are displayed with different color line.

higher Cr content on the UFS/NS surfaces [1,19]. This has already been revealed in many nano-grained stainless steels that a high density of grain boundaries in UFS/NS can promote the diffusion of Cr to a surface subjected to corrosion [1,20,21]. As further analyzed by Fig. 6, no corrosion pit is initiated around the ∑CSL boundaries (low-energy boundary). The observed corrosion pits are prone to be generated around the general high-energy boundaries (black line). Although these general high-energy boundaries can provide more pitting nucleation points, it also causes a higher driving force for Cr to diffuse to the surface subjected to corrosion [1,22], so as to form a thicker passive layer. This could indirectly verify the above assumption that high-energy boundaries may promote and enhance pitting resistance of HS sample. In the present work, the original metastable corrosion pits on HS sample surface propagate along all directions and often develop into stable corrosion pits in the RGs due to a small number of grain boundaries. When the propagating surface contacts with the interface between RG and UFS/NS, this propagating process could be suppressed by passive films from UFS/NS, just

leaving some mild corrosion pits on the HS sample surface (Fig. 2c). Thus, enhanced pitting resistance of the HS sample can be ascribed to the interrupted propagation of stable corrosion pits in RGs by the surrounded UFS/NSs.

4. Conclusions

In summary, the present heterostructured (HS) stainless steel with the mixed microstructures of recrystallized grains (RGs) and ultrafine/nano-structures (UFS/NSs) exhibited a significant enhancement of pitting resistance that the Ecorr was −8 mV and Icorr was 1.9×10^{-8} A·cm^{-2}. This enhanced pitting resistance was attributed to interrupted propagation of stable corrosion pits in RGs by surrounded UFS/NSs.

Declaration of Competing Interest

The authors declare no conflicts of interest.

Acknowledgments

The authors acknowledge the financial support of National Natural Science Foundation of China (51741106, 52071180), Natural Science Foundation of Jiangsu Province (BK20191292), Natural Science Foundation of Anhui Province (2008085J23), Project funded by China Postdoctoral Science Foundation (2020TQ0300), Natural Science Foundation of Anhui Provincial Education Department (KJ2020A0342), Foundation of Key Laboratory of National Defense Science and Technology (6142005180208) and the Scientific Research Starting Foundation of Anhui Polytechnic University of China (2020YQQ009, 2020YQQ026, 2020YQQ027).

REFERENCES

[1] Gupta RK, Birbilis N. The influence of nanocrystalline structure and processing route on corrosion of stainless steel: a review. Corros Sci 2015;92:1–15. https://doi.org/10.1016/j.corsci.2014.11.041.
[2] Lo KH, Shek CH, Lai JKL. Recent developments in stainless steels. Mater Sci Eng R 2009;65:39–104. https://doi.org/10.1016/j.mser.2009.03.001.
[3] Nasiri Z, Ghaemifar S, Naghizadeh M, Mirzadeh H. Thermal mechanisms of grain refinement in steels: a Review. Met Mater Int 2020. https://doi.org/10.1007/s12540-020-00700-1.
[4] Kwok CT, Cheng FT, Man HC, Ding WH. Corrosion characteristics of nanostructured layer on 316L stainless steel fabricated by cavitation-annealing. Mater Lett 2006;60:2419–22. https://doi.org/10.1016/j.matlet.2006.01.053.
[5] Jin ZH, Ge HH, Lin WW, Zong YW, Liu SJ, Shi JM. Corrosion behaviour of 316L stainless steel and anti-corrosion materials in a high acidified chloride solution. Appl Surf Sci 2014;322:47–56. https://doi.org/10.1016/j.apsusc.2014.09.205.
[6] Geng SN, Sun JS, Guo LY. Effect of sandblasting and subsequent acid pickling and passivation on the microstructure and corrosion behavior of 316L stainless steel. Mater Des 2015;88:1–7. https://doi.org/10.1016/j.matdes.2015.08.113.
[7] Hajizadeh K, Maleki-Ghaleh H, Arabi A, Behnamian Y, Aghaie E, Farrokhi A, et al. Corrosion and biological behavior of nanostructured 316L stainless steel processed by severe plastic deformation. Surf Interface Anal 2015;47:978–85. https://doi.org/10.1002/sia.5806.
[8] Punckt C, Bölscher M, Rotermund HH, Mikhailov AS, Organ L, Budiansky N, et al. Sudden onset of pitting corrosion on stainless steel as a critical phenomenon. Science 2004;305:1133–6. https://doi.org/10.1126/science.1101358.
[9] Williams DE, Kilburn MR, Cliff J, Waterhouse IN. Composition changes around sulphide inclusions in stainless steels, and implications for the initiation of pitting corrosion. Corros Sci 2010;52:3702–16. https://doi.org/10.1016/j.corsci.2010.07.021.
[10] Pan C, Liu L, Li Y, Wang FH. Pitting corrosion of 304ss nanocrystalline thin film. Corros Sci 2013;73:32–43. https://doi.org/10.1016/j.corsci.2013.03.022.
[11] Zheng ZB, Zheng YG. Effects of surface treatments on the corrosion and erosion-corrosion of 304 stainless steel in 3.5% NaCl solution. Corros Sci 2016;112:657–68. https://doi.org/10.1016/j.corsci.2016.09.005.
[12] Qin WB, Kang JJ, Li JS, Yue W, Liu YY, She DS, et al. Tribological behavior of the 316L stainless steel with heterogeneous lamella structure. Materials 2018. https://doi.org/10.3390/ma11101839.
[13] Li JS, Gao B, Huang ZW, Zhou H, Mao QZ, Li YS. Design for strength-ductility synergy of 316L stainless steel with heterogeneous lamella structure through medium cold rolling and annealing. Vacuum 2018;157:128–35. https://doi.org/10.1016/j.vacuum.2018.08.049.
[14] Li JS, Cao Y, Gao B, Li YS, Zhu YT. Superior strength and ductility of 316L stainless steel with heterogeneous lamella structure. J Mater Sci 2018;53:10442–56. https://doi.org/10.1007/s10853-018-2322-4.
[15] Li JS, Fang C, Liu YF, Huang ZW, Wang SZ, Mao QZ, et al. Deformation mechanisms of 304L stainless steel with heterogeneous lamella structure. Mater Sci Eng A 2019;742:409–13. https://doi.org/10.1016/j.msea.2018.11.047.
[16] Li JS, Mao QZ, Nie JF, Huang ZW, Wang SZ, Li YS. Impact property of high-strength 316L stainless steel with heterostructures. Mater Sci Eng A 2019;754:457–60. https://doi.org/10.1016/j.msea.2019.03.105.
[17] Yan FK, Tao NR, Pan C, Liu L. Microstructures and corrosion behaviors of an austenitic stainless steel strengthened by nanotwinned austenitic grains. Adv Eng Mater 2016;18:650–6. https://doi.org/10.1002/adem.201500368.
[18] Zhang C, Zhang ZW, Liu L. Degradation in pitting resistance of 316L stainless steel under hydrostatic pressure. Electrochim Acta 2016;210:401–6. https://doi.org/10.1016/j.electacta.2016.05.169.
[19] Liu L, Li Y, Wang FH. Influence of nanocrystallization on pitting corrosion behavior of an austenitic stainless steel by stochastic approach and in situ AFM analysis. Electrochim Acta 2010;55:2430–6. https://doi.org/10.1016/j.electacta.2009.11.088.
[20] Liu L, Li Y, Wang FH. Electrochemical corrosion behavior of nanocrystalline materials-a review. J Mater Sci Technol 2010;26:1–14. https://doi.org/10.1016/S1005-0302(10)60001-1.
[21] Pan C, Liu L, Li Y, Zhang B, Wang FH. The electrochemical corrosion behavior of nanocrystalline 304 stainless steel prepared by magnetron sputtering. J Electrochem Soc 2012;159:C453–60. https://doi.org/10.1149/2.034211jes.
[22] Fujita T, Horita Z, Langdon TG. Using grain boundary engineering to evaluate the diffusion characteristics in ultrafine-grained Al-Mg and Al-Zn alloys. Mater Sci Eng A 2004;371:241–50. https://doi.org/10.1016/j.msea.2003.12.042.